

Performance predictions of RF heated plasma in EAST

S Ding¹, B Wan¹, X Zhang¹, R V Budny², Y Guo¹, D McCune², P Xu¹,
J Yang¹, J Qian¹, Y Shi¹, F Wang¹ and S M Kaye²

¹ Institute of Plasma Physics, Chinese Academy of Sciences, Hefei, Anhui, 230031, People's Republic of China

² Princeton Plasma Physics Laboratory, Princeton University, Princeton, NJ 08543, USA

E-mail: archangel@ipp.ac.cn

Received 3 June 2010, in final form 21 October 2010

Published 23 November 2010

Online at stacks.iop.org/PFCF/53/015007

Abstract

Scenario development of high power L- and H-mode plasmas in the Experimental Advanced Superconducting Tokamak (EAST) tokamak is reported. The simulations use PTRANSP in combination with TSC to explore EAST plasmas with various radio frequency (RF) auxiliary heating methods, including ion cyclotron resonant heating (ICRH) and lower hybrid current drive. The GLF23 transport model is found to give a better fit to temperature measurements compared with the MMM95 and MMM08 models. A series of ICRH simulations are performed to optimize parameters of a new ICRH system in EAST. The highest plasma stored energy and other related plasma parameters using the current auxiliary power limits are predicted. The discharge length of high power plasma can be 8–200 s, depending on the volt-second consumption in different scenarios. Various phenomena are reported including the influence of different fractions of RF power on their deposition behavior, and on thermal diffusivity, the linear relation between q_0 and LHW power fraction, different behavior of fast ions between L- and H-mode plasmas. The scenario development is predicted to improve the performance of EAST.

(Some figures in this article are in colour only in the electronic version)

1. Introduction

After several successful campaigns of experiments and upgrades of internal structures and the radio frequency (RF) auxiliary heating system [1], Experimental Advanced Superconducting Tokamak (EAST) has the potential to achieve high power L-mode and even H-mode within the limit of current parameters. Studies of high power simulation including L-mode and H-mode boundary for EAST plasma are presented in this paper.

This study is the first to use the PTRANSP code to generate self-consistent time-dependent integrated predictions for EAST. PTRANSP [2] is the predictive upgrade of the TRANSP

code [3]. The prediction procedure starts with self-consistent total plasma current, 3D boundary etc, taken from the TSC code [4], with a presumed electron density profile. PTRANSP performs a detailed calculation of the plasma equilibrium, power deposition, transport and gives self-consistent results.

EAST is developing RF heating and current drive systems with 6 MW maximum power. This includes 4 MW of the ion cyclotron resonant heating (ICRH) system in the frequency range 25–70 MHz and 2 MW from the lower hybrid current drive (LHCD) system at 2.45 GHz frequency. Although the resonant double loop ion cyclotron resonant frequency (ICRF) antenna with two straps can be operated with different phasings for various scenarios, in this study they are kept the same, $n_{\parallel} = 23$, which means the phasing is 180° . The multi-junction coupler of the LHCD system can launch the LHCD power with parallel refractive index n_{\parallel} from 1.6 to 3.2 and typical FWHM of 0.2 at $n_{\parallel\text{peak}} = 2.3$ [1]. In this study, the parallel refractive index $n_{\parallel\text{peak}}$ is fixed at 2.1.

These simulations provide insight into the possibility of achieving H-mode, and thus are important for the high power scenario development. The predicted plasma parameters can help physicists design their proposals. This study will be further compared with experiments in EAST to test theoretical transport models in PTRANSP.

In section 2, the target plasmas are discussed as well as the modeling details. Results of ICRH simulation are shown in section 3. With the optimized ICRF parameters, high power EAST simulations are carried out and the results are then given in section 4. Conclusion of this paper is presented in section 5.

2. Target plasma and modeling details

Presently PTRANSP is a fixed boundary code. The boundary evolution and initial electron temperature profile are taken from the output of the TSC code, which simulated a reference shot from the EAST database. The reference shot (shot# 12755) was selected from the EAST spring campaign in 2009. Its basic parameters are double null, $I_p = 500$ kA, $B_T = 2$ T at 175 cm, line-averaged density $\bar{n}_e = 2.1 \times 10^{19} \text{ m}^{-3}$, $P_{\text{LHW}} = 450$ kW, $Z_{\text{eff}} = 3.1$. Since there are no measured density profile data, the profile is assumed to have an L-mode boundary (figure 1), which roughly fits the three channels of line-averaged density measurements (shot# 12755) along different chords, respectively, located at $R = 1.64$ m, 1.82 m and 2.00 m, and is used both in TSC and PTRANSP runs. Here ρ is a magnetic flux coordinate defined as the square root of the normalized toroidal flux ($\sqrt{\Phi/\Phi_a}$). A comparison between two time slices of EAST discharge (shot# 19939), which are with ICRH on (3.4 s) and with LH heating only (3.85 s), shows the densities in three channels increase 22%, 21% and 17%, respectively. The increments are quite close, which means EAST density profile may not change very much in the LH heating phase and in the ICRH phase. Thus, in this study, for the sake of simplicity and eliminating effects of varying density profiles on plasma features, the same density profile is used in both LH heating and ICRH scenarios. H-mode discharge is not yet achieved in EAST. In figure 1, the assumed H-mode boundary density profile is inferred from the reports of other tokamaks [5–7]. Density profiles of both L- and H-mode boundary used in this prediction study are scaled up and down, respectively, if the required line-averaged density is different from $2.0 \times 10^{19} \text{ m}^{-3}$ in figure 1.

The time-dependent solutions of plasma equilibrium are computed using the TEQ code [8] in PTRANSP. Several theoretical transport models had been tested in PTRANSP runs, while x-ray crystal spectrometer (XCS) gave electron and ion temperature profiles and electron temperature experiment data were also provided by soft x-ray pulse height analysis (SXPHA) (figure 2(a)). Further, three Ohmic shots with different line-averaged densities were also

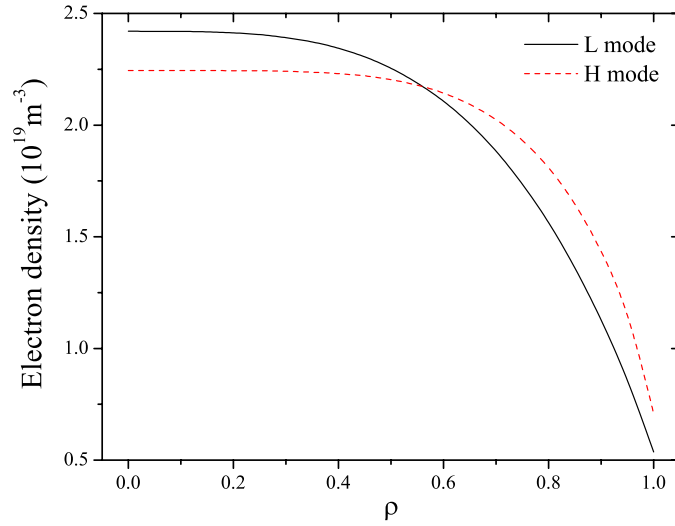


Figure 1. Density profiles for L- (solid line) and H- (dashed line) mode boundary used in this study. The profile of L-mode fits measurements for shot# 12755, and the H-mode profile is inferred from the reports of other tokamaks. The line-averaged values in this figure are both $2.0 \times 10^{19} \text{ m}^{-3}$.

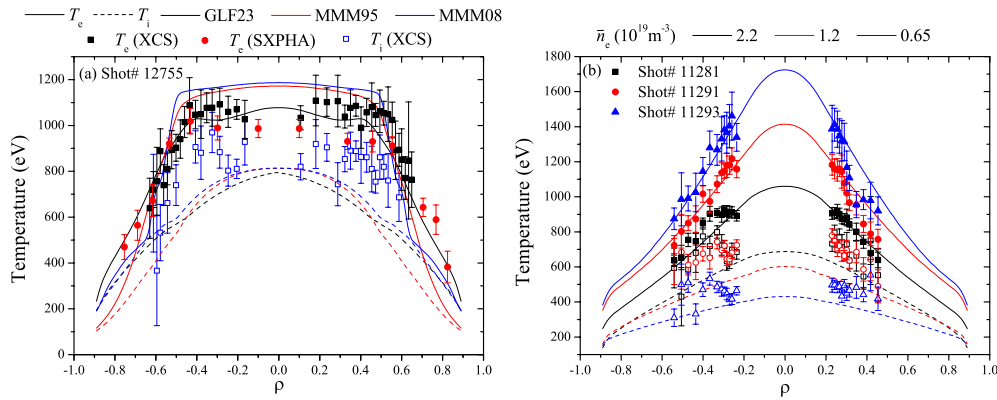


Figure 2. (a) Comparison of calculated temperature profiles from different theoretical models (lines in different colors, and solid lines for electron temperature, dashed lines for ion temperature) and experiment data (solid dots for electron temperature and open dots for ion temperature). (b) TRANSP fits (lines) and experiment data (dots) of Ohmic shots with different line-averaged densities (in different colors) using GLF23 in combination with the Chang–Hinton model. The meaning of the other symbols is the same as in (a). (Color online.)

simulated as benchmark against experiment data (figure 2(b)). The PTRANSP result is mapped from one-sided data to two-sided profile in these figures, for the original PTRANSP data are flux-averaged. For now, neutral beams (NBs) are the only external torque source in PTRANSP. Since no beams are yet present in EAST, plasma rotation is assumed to be zero in this study. Thus, the stabilization effect of the $E \times B$ shear on turbulence, especially in the ion channel, is lost. In consequence, the predictive ion temperature is expected to be lower than the experiment result. The difference in ion temperature can reach 25–35% according to the previous study [9] in strong NB heated plasma. Not only NB but also RF heating can drive flows toroidally and poloidally [10, 11]. Intrinsic rotation and rotation driven by RF heating may be low in

comparison with that of NBI, so the predictive ion temperature in this study can perhaps be about 10% lower than the results with actual rotation in the EAST plasma driven by the RF power. Nevertheless, the stiff GLF23 model [9, 12] (with the Chang–Hinton model in the plasma core region) fits the experiment data best in comparison with MMM95 [13] and MMM08 [14] models. GLF23 model was chosen for high power EAST simulation in this study.

In this study, the plasmas of 500 kA plasma current and double null configuration were studied. The toroidal field was usually set to 2 T at 175 cm and can be scaled down to 1.8 T or up to 2.56 T in some runs for comparison. According to the PEDESTAL module [15], the L–H transition power varies from 1.0 to 1.8 MW depending on the line-averaged density, which was varied from 1.5 to $3.0 \times 10^{19} \text{ m}^{-3}$, and the toroidal field. Two ICRF heating regimes were studied, including ^3He minority heating (MH) and H second harmonic (SH) heating in D plasma. The concentration of H ($n_{\text{H}}/n_{\text{e}}$) was set to 20%, considering the reality of EAST wall conditioning, which has high hydrogen retention and high wall recycling. Carbon is considered as the primary impurity. In the situation of $Z_{\text{eff}} = 3.1$, which is used in this study, the carbon concentration ($n_{\text{C}}/n_{\text{e}}$) is about 7%, while $n_{\text{C}}/n_{\text{ion}}$ is about 10%. As we know, it is not possible to extract all the RF source power into the plasma, and transfer and coupling loss exists. The possible maximum effective auxiliary power for current EAST parameters is assumed to be $2 \text{ MW (ICRF)} \times 0.7 + 1.2 \text{ MW (LHW)} \times 0.85 = 2.4 \text{ MW}$. The multipliers are due to transfer loss and coupling loss. The predicted radiated power in PTRANSP is far below the realistic level. Lacking radiation data for the EAST experiment, the fraction of radiated power was assumed to be from 30% to 50% of total injected power in this work. Therefore, the maximum effective auxiliary power used in PTRANSP runs was set to 1.7 MW, while $P_{\text{ICRF}} \leq 1.4 \text{ MW}$, $P_{\text{LHW}} \leq 1.0 \text{ MW}$.

The RF heating and current drive system is the only auxiliary heating method in EAST at present. In PTRANSP runs, the TORIC full wave code [16] is used to model the ICRF heating process. In this paper, poloidal modes are 63, thus, the number of poloidal mesh points is 128. Besides, the number of radial mesh points is 323. Symmetric n_{\parallel} spectra of $n_{\parallel} = 23$ are used with the real antenna geometry in EAST. The effect of 2.45 GHz LHCD can be simulated by the LSC code [17] in PTRANSP. The phasing of the LH coupler is 0° in this study.

3. ICRH simulation

ICRH would play a critical role in EAST experiment not only in the future but also at present. Optimizing ICRH parameters is necessary for further EAST high power simulation. This set of ICRH simulations is designed on a low level of ICRF power (400 kW) and medium density ($2.0 \times 10^{19} \text{ m}^{-3}$, mostly), using the L-mode density profile in figure 1, to find the dependence of ICRF power deposition feature on various plasma parameters. During each scan, the plasma equilibrium and configuration change little.

3.1. ^3He MH in D plasma

It is well known that ICRF MH using ^3He in D plasma has high absorption efficiency in thermal ion heating in comparison with other ICRH regimes used in tokamaks. The baseline scenario for ITER also uses ^3He MH in DT plasmas. At present, it is capable of conducting ^3He MH in EAST in order to obtain good heating effect especially in the ion channel. In this simulation, some features of ^3He MH plasma are summarized with real EAST parameters. The frequency range of the current ICRF system is 25–70 MHz. 25 MHz is used for ^3He MH in this simulation.

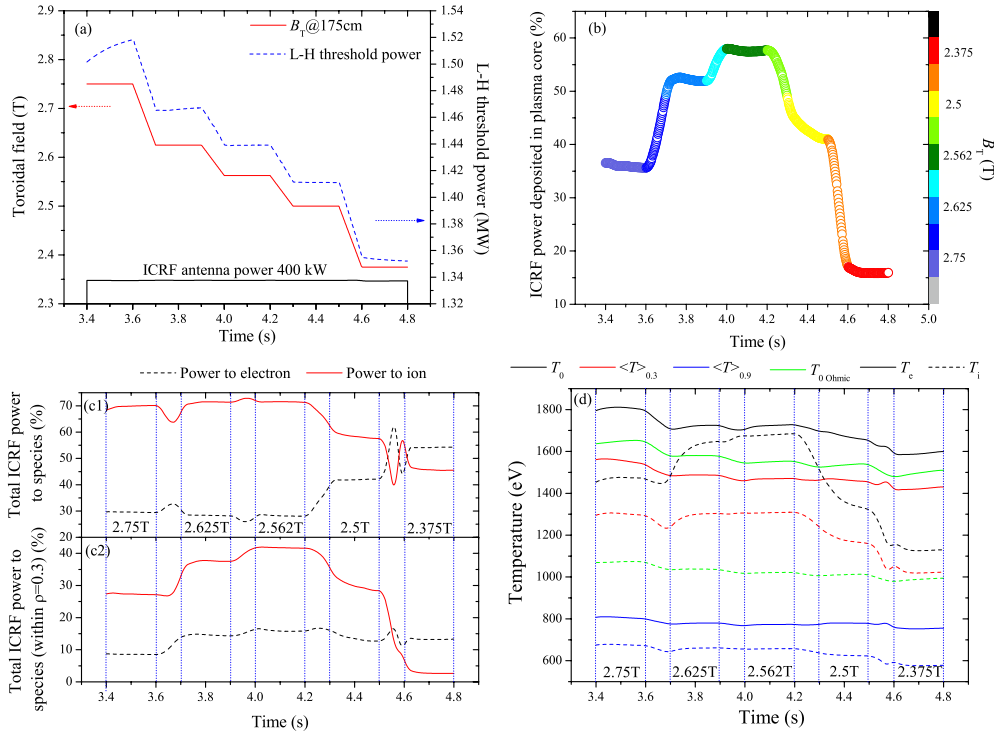


Figure 3. Results of B_T scanning in ICRF ^3He MH plasma. The line-averaged density is $2.0 \times 10^{19} \text{ m}^{-3}$. Minority concentration is 3%. (a) The waveform of ICRF power, B_T , and its related L–H transition threshold power. (b) The ratio of ICRF power deposited in plasma core ($\rho \leq 0.3$) to total ICRF power. The color coding is the evolution of B_T . (c) ICRF power deposited on the bulk plasma species, after fast ion thermalization. (c1) shows the global effect, while (c2) shows the core region. (d) Time history of temperature. The black line indicates temperature at axis. The red line is the volume-averaged temperature from axis to $\rho = 0.3$, while the blue line shows the global effect, which is volume-averaged within $\rho = 0.9$. The green line shows the temperature at axis in the Ohmic case with other input parameters unchanged in order to show the effectiveness of ICRF heating. (Color online.)

Figure 3 shows the results of B_T scanning in ICRF ^3He MH plasma with constant ^3He concentration of 3%. The ICRF power is kept constant during the scanning. B_T scans from 2.37 to 2.75 T. Its related L–H transition threshold varies from 1.35 to 1.52 MW accordingly (figure 3(a)). A disadvantage of using ^3He MH is the increase in L–H threshold power, because the toroidal field is usually 2 T in the EAST experiment for now. It is hoped that the high efficiency of ^3He MH can compensate this disadvantage in the experiment. When B_T is larger than 2.5 T, the total thermal ion heating effect becomes saturated (figure 3(c1)). However, the core plasma heating effect still changes. It is found that the best core plasma heating effect appears around $B_T \sim 2.56$ T (figures 3(b) and 3(c2)). The heating effect can also be seen from the time history of temperature (figure 3(d)). The resonance position in this case is about 6 cm at high field side from the axis. The absorption peak of ICRF power is at about $\rho = 0.17$. The slight off-axis heating makes more power depositing in the plasma core region (large plasma volume) rather than the exact on-axis heating (small plasma volume).

Similarly, minority scanning is also performed. Based on the result of B_T scanning, B_T is set to 2.56 T in this scanning. In figure 4(a1), when minority concentration is larger

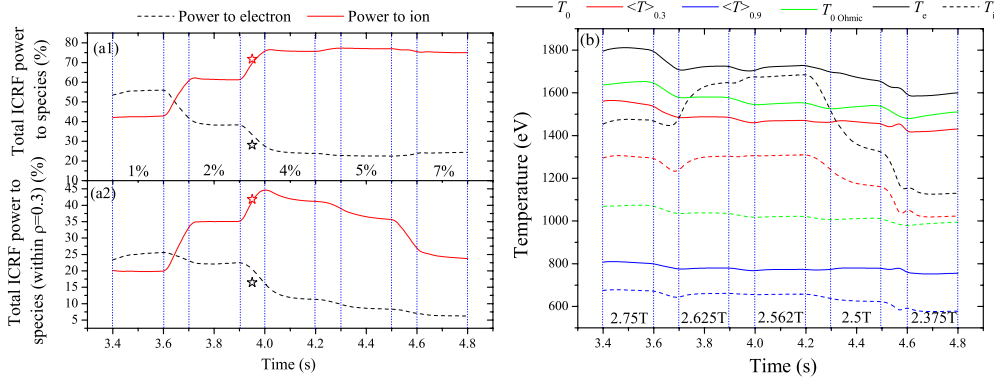


Figure 4. Results of minority concentration scanning in ICRF ^3He MH plasma. Based on the result of B_T scanning, B_T is set to 2.56 T. (a) ICRF power deposited on different thermal plasma species. (a1) Global power deposition. (a2) Power deposition in plasma core region ($\rho \leq 0.3$). The stars indicate the data of $n_{\text{min}}/n_e = 3\%$ in the previous B_T scanning. (b) Time history of temperature. Similar line types and colors are used as in figure 3. (Color online.)

than 4%, ICRF power deposited on global ions is saturated. However, the power deposited on ions in the plasma core region then starts to fall. The temperature reflecting the heating effect also shows this trend (figure 4(b)). The optimized minority concentration may be 4%, for good ion heating effect and fair electron heating effect. Detailed comparison between low minority concentration (2%), medium concentration (4%) and high concentration (7%) shows that when minority concentration varies from 2% to 4%, the increase in ion heating effect is because minority species transfer more power to thermal ions in the process of thermalization. However, the reason for the decrease in ion heating as well as electron heating when minority concentration varies from 4% to 7% is that minority species gain less ICRF power within the plasma core region, i.e. there is an outward shift of the minority species absorption peak.

Plasma density scanning from 1.5 to $3.0 \times 10^{19} \text{ m}^{-3}$ (line-averaged density) is then tested using $B_T = 2.56 \text{ T}$ and $n_{\text{min}}/n_e = 4\%$. It is found that high density is good for global ion heating in this ICRF regime (figure 5(a1)) and density has strong influence on ICRF power deposition profile (figure 5(a2), ICRF power deposited in the plasma core region varies.). The possible reason may be that at low density (figure 5(b)), minority particles can reach very high temperature, e.g. 10 keV or higher in the center when accelerating by E field in this case. This temperature mentioned here is the equilibrium temperature, for the TORIC code treats any fast ions as a special ion species with an equivalent Maxwellian distribution. Thus, the Doppler effect of resonance is strong compared with high density cases, making ICRF power strongly absorbed near the plasma core. When the density becomes higher (figure 5(c)), the Doppler effect is quite small because of the lower minority temperature. Part of the minority particles gains energy along the Z direction at resonance position rather than in the plasma core, causing the outward shift of the absorption peak. If the density is even higher (figure 5(d)), the degradation of the Doppler effect becomes saturated. Meanwhile, the absorption efficiency of single pass increases as density increases. More power is absorbed when the wave is injected into the plasma core region. The region of power absorption is not that scattered along the Z direction compared with figure 5(c), which causes the result of inward shift of absorption peak in the power deposition profile. It is found that mode conversion also plays a role in the power deposition, especially in the case of $2.5 \times 10^{19} \text{ m}^{-3}$.

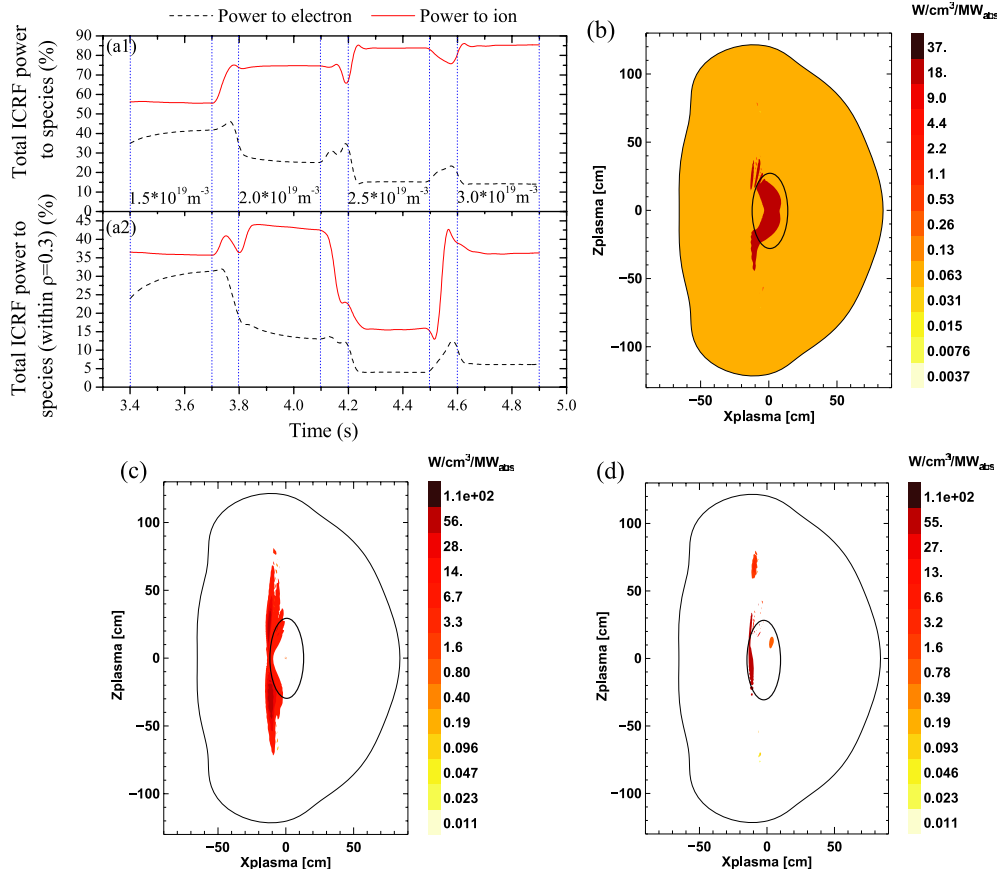


Figure 5. Results of plasma density scanning. Based on previous scanning, $B_T = 2.56 \text{ T}$ and $n_{\text{min}}/n_e = 4\%$. (a) ICRF power deposited on different thermal plasma species. (a1) Global power deposition. (a2) Power deposition in plasma core region ($\rho \leq 0.3$). (b)–(d) 2D diagrams of ICRF power deposition on ^3He (minority) with different line-averaged densities. The dashed line indicates the contour corresponding to $\rho = 0.3$. (b) $2.0 \times 10^{19} \text{ m}^{-3}$, (c) $2.5 \times 10^{19} \text{ m}^{-3}$, (d) $3.0 \times 10^{19} \text{ m}^{-3}$. (Color online.)

3.2. H SH heating in D plasma

Hydrogen SH heating is another choice for EAST ICRH regime, which can be conducted in relatively low toroidal field to reduce the L–H threshold power. Hydrogen MH is hard to apply due to the reality of EAST wall conditioning and high hydrogen retention. In this simulation, B_T is set to 2 T and ICRF varies from 52 to 62 MHz. It is found that when the frequency is 58 MHz, the plasma has best response to ICRF heating, i.e. best thermal ion heating effect, especially in the plasma core region, and fair electron heating effect (see figure 6).

With varying density, very different ICRF power absorption behavior in hydrogen SH heating plasma is observed in comparison with that in the MH case. The simulation was conducted with ICRF 58 MHz and 2 T toroidal field in the target plasma. In figure 7(a1), if density is too low, the fraction of global ICRF power to ions is also low. A gradually increasing density will lead to gradually higher global ICRF power deposition fraction on ions, which is similar to the MH case in figure 5. However, the time history of power deposition within

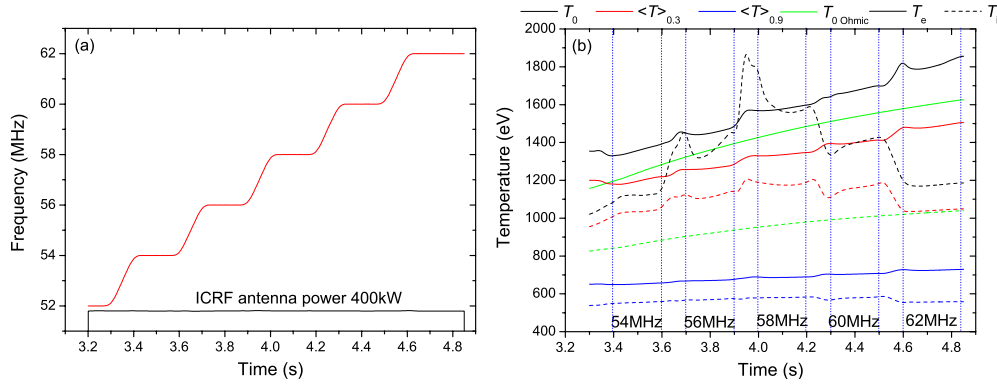


Figure 6. Results of frequency scanning in ICRF hydrogen SH heating plasma. The typical plasma parameters of $B_T = 2\text{ T}$ and $\bar{n}_e = 2.0 \times 10^{19}\text{ m}^{-3}$ are used in this simulation. (a) Waveform of ICRF antenna power and ICRF. (b) Time history of temperature. Similar line types and colors are used as in figure 3. (Color online.)

$\rho = 0.3$ is quite different from the MH case. When density is evolved to $2.5 \times 10^{19}\text{ m}^{-3}$, a large percentage of ICRF power is deposited in the plasma core region in the SH case, which means an inward shift of absorption peak in contrast to the peak outward shifting in the MH case in figure 3.

The detailed comparison of 2D ICRF power deposition on hydrogen is shown in figures 7(b)–(d). Unlike the cases in the MH regime, the power deposition regions are similar, located between $+70$ and -70 cm along the Z direction at the resonant layer in different density SH cases. However, the power densities in this region along the Z direction are different in each SH case. In figure 7(b), the peak of power density is at ± 20 cm, and the averaged power density in the region from 20 to 45 cm is higher than the plasma core region (around 0 cm). The result is only 30% of the total ICRF power deposited within $\rho = 0.3$. When the density is higher, the phenomenon is that the peak of power density moves toward the plasma core at about ± 7 cm with a high peak value in comparison with that of other cases. The power density distributes sparsely in the region of $|Z| > 15$ cm (figure 7(c)). There is more than 65% of total ICRF power deposited within $\rho = 0.3$, which also causes very good core heating effect and high central ion temperature. In figure 7(d), the line-averaged density is $3.0 \times 10^{19}\text{ m}^{-3}$ and the power density in the region of $|Z| < 25$ cm is obviously higher than that of the outer region. In the SH regime, the absorption efficiency of single pass is related to ion beta, which means not only density but also ion temperature would have influence on the absorption of ICRF power. According to the TORIC output, in the case of $2.5 \times 10^{19}\text{ m}^{-3}$, the hydrogen central thermal pressure is even slightly higher than that of the high density case of $3.0 \times 10^{19}\text{ m}^{-3}$. More power is absorbed when the wave is injected into the plasma core region if the absorption efficiency is high. Different absorption efficiencies are possibly the reason for inward and outward shifting of the absorption peak. Moreover, there is no strong Doppler effect observed in the SH regime, which is because TORIC does not include the interaction between hydrogen SH resonance and ion hybrid resonance. Further investigations are under way to better understand the effect of density on the power deposition.

4. High power EAST simulation

With the knowledge of ICRF simulation, high power EAST simulation is then performed using the parameters in table 1. Low power H-mode simulates the plasma without an excellent heating

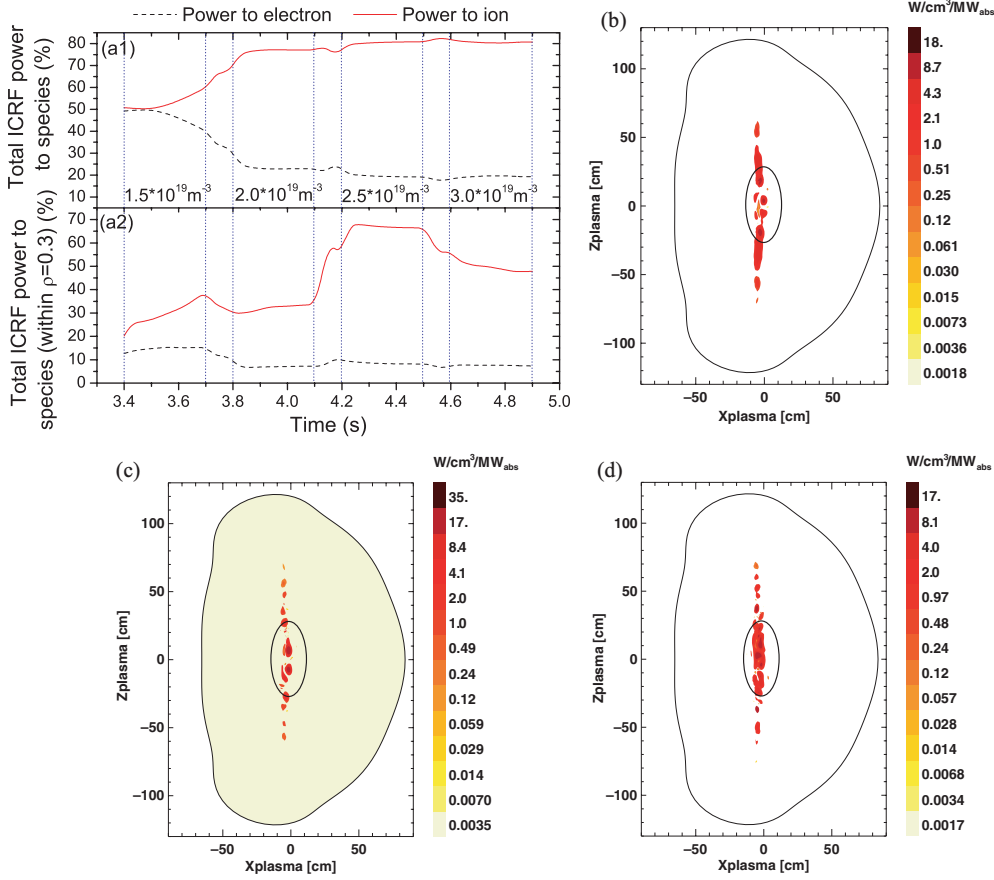


Figure 7. Results of plasma density scanning in ICRF hydrogen SH heating plasma. Based on previous scanning, $f = 58$ MHz and $B_T = 2$ T. (a) ICRF power deposited on different thermal plasma species. (a1) Global power deposition. (a2) Power deposition in the plasma core region ($\rho \leq 0.3$). (b)–(d) 2D diagrams of ICRF power deposition on thermal ions (hydrogen) with different line-averaged densities. The dashed line indicates the contour corresponding to $\rho = 0.3$. (b) $2.0 \times 10^{19} \text{ m}^{-3}$, (c) $2.5 \times 10^{19} \text{ m}^{-3}$, (d) $3.0 \times 10^{19} \text{ m}^{-3}$. (Color online.)

Table 1. Parameters used in high power EAST simulation.

Scenario	I_p (kA)	B_T (T)	\bar{n}_e (10^{19} m^{-3})	P_{aux} (MW)	P_{L-H} (MW)	ICRH regime/ f (MHz)
L-mode	500	2, 2.56	1.5–3	0.6	—	SH/58, MH/25
H-mode	500	1.8, 2	1.5, 2	0.9, 1.2	0.9–1.18	SH/58
H-mode	500	2.56	1.5–3	1.7	1.22–1.8	MH/25

effect and the plasma with high radiated power (50%) as well (so the effective heating power simulated in PTRANSP is artificially lowered). High power H-mode simulates the plasma with good heating and relatively low radiated power (30%). The last column in table 1 shows the different ICRH regimes and their frequencies used in different scenarios. The ICRH regimes SH and MH stand for H SH heating and ^3He MH, respectively. In this set of simulations, the ^3He minority concentration (n_{min}/n_e) is set to 4%, which is the optimized value determined in section 3.1, and the concentration of hydrogen (n_{H}/n_e) in deuterium plasma is 20% as

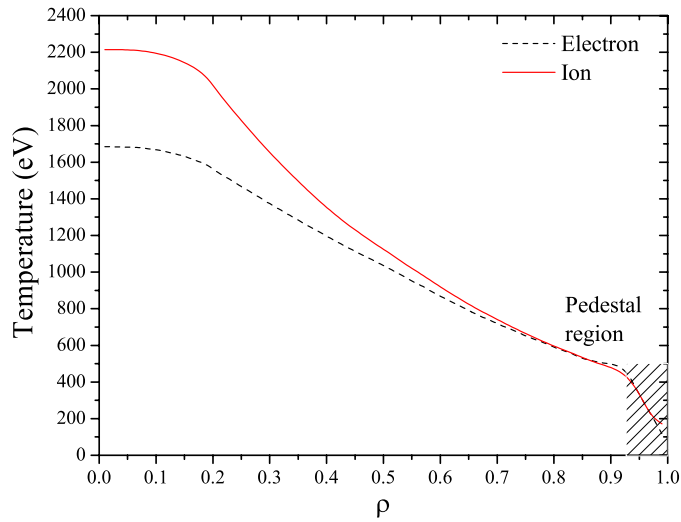


Figure 8. Temperature profiles of the plasma with the highest stored energy.

mentioned in plasma modeling in section 2. Toroidal field varies to meet the requirement of different ICRH regimes. If the heating effect is not really good or the radiated power is too high, EAST can also be operated in $B_T = 1.8$ T and line-averaged density $\bar{n}_e = 1.5 \times 10^{19} \text{ m}^{-3}$, which only requires $P_{L-H} = 0.9$ MW, according to the PEDESTAL module. Same auxiliary heating power has different combinations of ICRF and LHW power. The influence of different combinations of RF power on plasma feature will be shown.

Simulations in section 3 have one time-dependent-varying parameter in each run, while each run in this section has constant parameters. That is because it is found that lower hybrid wave had complicated interaction with q profile. Other parameters such as plasma density, electron temperature affect the interaction between them. A LHW injected run with increasing plasma density may have different q profiles in comparison with another run with decreasing plasma density, although the lowest and highest densities in these two runs are the same. GLF23 predictions depend sensitively on q profiles. This result provides a possible way to adjust the absorption of LHW and the evolution of q profile in different density conditions to achieve better plasma performance. However, it will not be further discussed in this paper. It is difficult to find differences between the constant-parameter runs and the varying-parameter runs in ICRH simulations. High power EAST simulation usually includes both ICRF and LHW auxiliary heating. It is clear that simulations in this section should use constant parameters in each run to avoid the ‘memory’ effect.

In this set of simulations, the highest stored energy in the plasma that can be possibly achieved in current parameters is about 155 kJ. The temperature profiles of this run are shown in figure 8. The pedestal height is 440 eV for both electron and ion temperature profiles, and the pedestal is located at about $\rho = 0.92$. Some related parameters are line-averaged density $\bar{n}_e = 3.0 \times 10^{19} \text{ m}^{-3}$, based on the H-mode profile in figure 1, effective total heating power $P_{\text{heat}} = 1.9$ MW, including lower hybrid wave power $P_{LH} = 300$ kW, ICRF power $P_{ICRF} = 1.4$ MW, using ^3He MH with $n_{\text{min}}/n_e = 4\%$. Ohmic heating also contributes approximately 200 kW to the total heating power. Further, $\tau_E = 74$ ms, $H_{98} = 1.05$, $\beta_N = 0.66$. In the near future, when 6 MW total source power is available, EAST plasma may store 40% extra energy than the maximum energy in this campaign. After calculating the

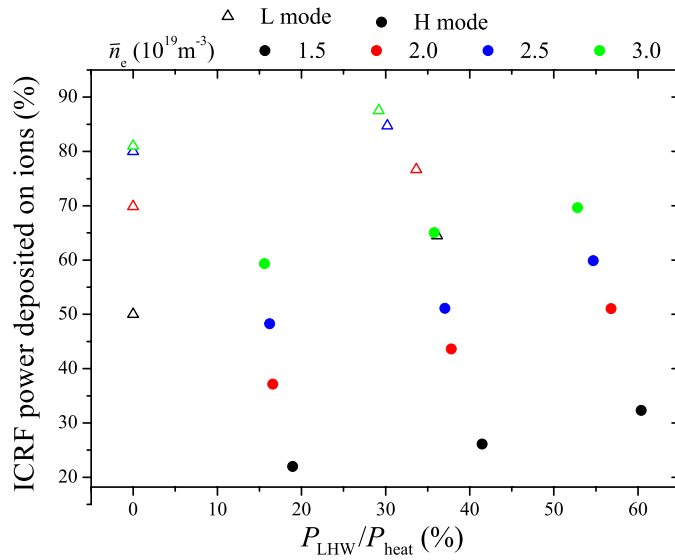


Figure 9. Fraction of lower hybrid power has an influence on ICRF power deposition on plasma species. Circular dots show H-mode data, while triangular dots indicate L-mode data. Data in different plasma densities are shown in different colors. (Color online.)

volt-second consumption and the initial volt-second provided by the TSC code, the possible discharge length of high power plasma in this set of simulation will be 8–200 s, depending on different scenarios of RF power combinations. Note that in this set of simulations, the total auxiliary heating power is selected to be several levels, which are shown in table 1. In each power level, different combinations of RF power (different ratios between ICRF and lower hybrid power) are tested. In the following part of this section, plasma features due to the RF power variation are introduced. Total heating power is generally considered as a critical factor that affects plasma feature, while there is not much discussion about the effect of different RF power combinations on plasma feature. Thus, some results in this section are discussed in terms of the ratio of ICRF or LHW power to the total heating power. The different effects between ICRF and lower hybrid power on plasma features are therefore shown, in the cases where similar total heating power is maintained.

4.1. ICRF power deposition on thermal ions

The combination of RF power has an influence on ICRF power deposition (the MH regime) on thermal plasma species (figure 9), although plasma density and boundary condition (L- or H-mode) are the major factors. The influence of density is clearly identified in figures 5(a) and 7(a). This effect can also be seen in figure 9. Besides, the fraction of ICRF power on thermal ions can be quite different (20% in high density and 40% in low density) between L- and H-modes even at the same line-averaged density condition. The influence of RF power combination is not that strong in comparison with density and boundary condition. The difference shown in figure 9 is about 5–15%. In the ^3He MH regime, ICRF power does not deposit on thermal ions directly. Minority species get the power first, and then transfer the power to thermal ions via thermalization. Detailed analysis shows that more ICRF power (about 10% of its total power in the high density case and 20% in the low density case) can be deposited on minority species in the L-mode than that in the H-mode plasma. RF power combination has

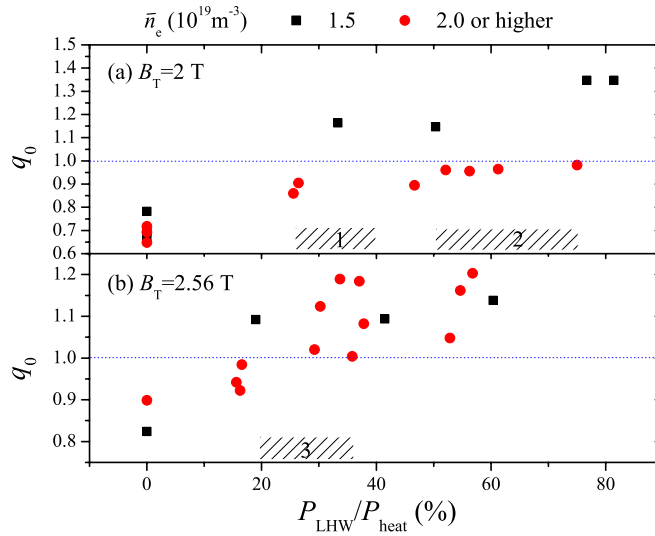


Figure 10. The influence of lower hybrid wave power on q_0 . Black squares are low density data, while red circles are high density ($\geq 2.0 \times 10^{19} \text{ m}^{-3}$) data. Shaded region indicates the so-called critical fraction of LHW power to make $q_0 > 1$. #1 and #2 are for low and high density data in (a), respectively. #3 is for high B_T data in (b).

no effect in this phase. Besides, in the process of fast ion thermalization, minority species can transfer more power (as much as 20% of minority species power in the high density case and 40% in the low density case) to thermal ions in the L-mode plasma than that in the H-mode plasma. Varying RF power combination shows a difference of about 10–25% in this phase. It is clear that the major change of deposited ICRF power fraction on thermal ions is in the process of fast ion thermalization. In this simulation, one major difference between L- and H-mode boundary conditions can be considered as the change in density profiles. L-mode has higher plasma density in the plasma core region than that of the H-mode if the line-averaged density is the same (figure 1). Meanwhile, the peak of absorbed ICRF power density is close to the plasma center. Another major difference is that the H-mode simulation has higher total heating power level (1.8 MW) than that of the L-mode (0.9 MW). In the process of fast ion thermalization, similar to the NBI case, the electron heating fraction by minority particles is proportional to the minority energy and inversely proportional to the electron temperature. High ICRF power increases minority energy. Low density also increases minority energy, which can be obtained from the TORIC output. These two conditions all increase electron heating fraction by minority particles, while decreasing the final ICRF power deposited on thermal ions. Therefore, the reasons for difference due to density and RF power combination are straightforward. The difference of L- and H-mode conditions may be partially because of the different power levels, and partially because of the different central densities.

4.2. Central q value

In the EAST plasma, a nearly linear relation between q value at axis (q_0) and the ratio of LHW power to total heating power is obtained (figure 10). The so-called critical fractions of LHW power, which can make $q_0 > 1$, in order to avoid sawtooth phenomenon in plasma core region, are identified in different parameters. In low toroidal field cases, low plasma density ($1.5 \times 10^{19} \text{ m}^{-3}$) has low critical fraction at about 35%, i.e. shaded region #1 for black squares

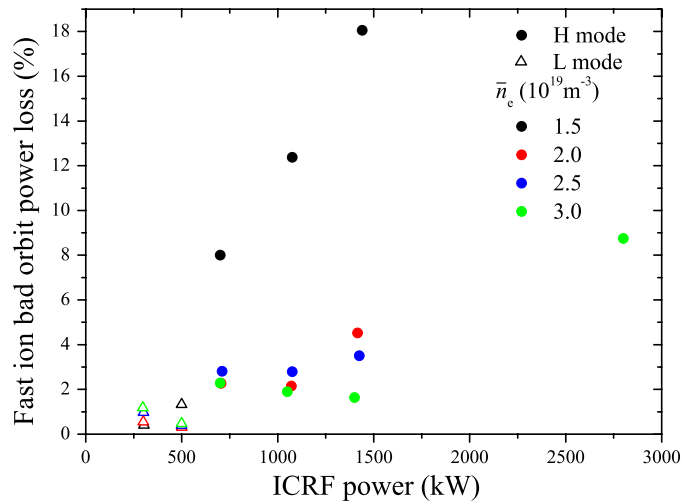


Figure 11. Fast ion bad orbit power loss (normalized by ICRF power) versus ICRF power. Circular dots are H-mode data, and triangular dots are L-mode data. Different colors indicate different plasma densities. (Color online.)

in figure 10(a). When the density becomes higher, the critical fraction is also larger. A fraction in the range 55–75% may be required for the plasmas with density larger than $2.0 \times 10^{19} \text{ m}^{-3}$ (shaded region #2 for red circles in figure 10(a)). In high toroidal field cases, density does not separate the trend. The critical fraction is around 25% (shaded region #3 in figure 10(b)). The importance of using ratio of lower hybrid power to total heating power is because in simulation, it is observed that the Ohmic current density can be enhanced by ICRF power injection locally around the deposition location, which is usually in the plasma center. The result is that the local q (or q_0) would decrease. Therefore, only considering ‘ q_0 versus P_{LHW} ’ is not enough to reveal this phenomenon, while taking RF power fraction into account this phenomenon is revealed quite well.

4.3. Fast ion bad orbit power loss

Fast ion bad orbit power loss calculated in PTRANSP can be significant in low density H-mode runs with high ICRF power (figure 11). Because the quantity in the y -coordinate had already been normalized by the total ICRF power, the fast ion bad orbit power loss in the case of low density ($1.5 \times 10^{19} \text{ m}^{-3}$, black circular dots in figure 11) actually has a quadratic increasing trend when ICRF power increases. It is important to operate EAST with high density if the auxiliary heating system is further developed in the near future. Bad orbit loss in L-mode seems less significant, can even be negligible, not only because the ICRF power injected into the plasma is not high, but also for lower increase trend in comparison with that in H-mode cases.

4.4. Thermal diffusivity

χ also is related to the ICRF power, especially the χ in the plasma core region. In figure 12(a), it is clear that the ICRF power significantly enhances electron thermal diffusivity in the plasma core region. A similar phenomenon is observed in the ion channel. As mentioned in the previous section, in this simulation, ICRH focuses on optimized ion heating effect, as well as

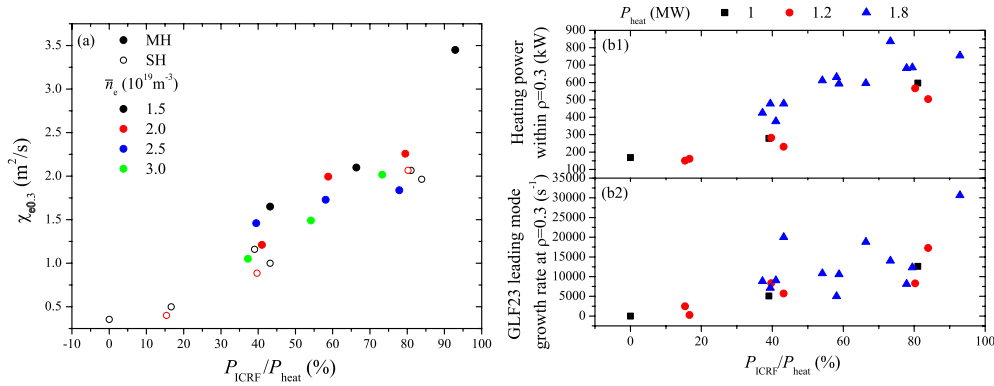


Figure 12. (a) χ_e at $\rho = 0.3$ versus fraction of ICRF power. Solid dots are ^3He MH data, and open dots are H SH heating data. Different colors indicate different plasma densities. (b) Heating power deposited in the plasma core region and GLF23 leading mode growth rate versus ICRF power fraction. Data with three total heating power levels are involved. The squares are for 1 MW. The circles and triangles are for 1.2 MW and 1.8 MW, respectively. (Color online.)

plasma core heating effect. Higher fraction of ICRF power indicates higher power is injected into the plasma core region (figure 12(b1)), because in this simulation, LHW power is usually deposited in the region of $0.4 \leq \rho \leq 0.6$. In figure 12(b1), the total heating power deposited in the plasma core region ($\rho \leq 0.3$) increases almost linearly as the fraction of ICRF power increases. Meanwhile, turbulence is excited. There is no available EAST model in nonlinear gyrokinetic code, such as GYRO or GS2. The growth rate of leading mode calculated by GLF23 is therefore shown in figure 12(b2) to provide the basic insight into the influence of heating power on turbulent instability. In this figure, growth rate at $\rho = 0.3$ increases when the fraction of ICRF power increases, i.e. the heating power deposited in the plasma core region increases. The trends for low and high total heating power cases are similar. No distinct difference can be observed. Due to the absence of rotation, no $E \times B$ shear stabilization is working to suppress the growing turbulence. The anomalous thermal diffusivity is mainly determined by the growth rate of leading mode calculated by GLF23. The frequencies of leading mode usually are in the range 200–450 kHz. They are in the typical temporal scale of ITG and dissipative TEM. Thus, ITG and/or (D)TEM may be responsible for the rise in thermal diffusivity when heating power increases. Regarding χ_s in outer radius, e.g. $\rho = 0.65$, such a monotone increasing trend is very weak, because the power injected into this volume does not change much if total auxiliary heating power is fixed.

5. Conclusion

In this paper, PTRANSP in combination with TSC has been firstly applied on EAST simulation. After benchmarking against the experiment data, the GLF23 model (with Chang–Hinton model in the plasma core region) is found to fit the experiment data best and is selected for the further simulation. The presumed density profile in the PTRANSP simulation in this work is from a real LH case for the L-mode study, while scaling it up or down to obtain different desired line-averaged densities. For the H-mode cases, the density profile is assumed and shown in figure 1 along with the L-mode density profile. A set of parameter scanning simulations are performed for different ICRF heating regimes, which is new for the EAST experiment. The optimized parameters are obtained in currently used plasma equilibrium and configuration

and are further used in high power EAST simulation, which uses real EAST parameters for scenario development. In the ^3He minority heating regime, the optimized parameters are $B_T = 2.56\text{ T}$, $f = 25\text{ MHz}$, $n_{\text{min}}/n_e = 4\%$, while in the hydrogen second harmonic heating regime, the optimized parameters are $B_T = 2\text{ T}$, $f = 58\text{ MHz}$. The different ICRF power deposition results in density scanning are briefly discussed. The Doppler effect and single pass absorption efficiency are major factors that affect the power deposition. In this set of high power EAST simulations, the possible achieved highest plasma parameters are shown, including stored energy (155 kJ), line-averaged density ($3.0 \times 10^{19}\text{ m}^{-3}$), temperature profiles and so on. Further, various plasma features related to RF power combinations are observed and briefly discussed. The difference between ICRF and lower hybrid wave power, which is mainly because of their different deposition positions, may affect many aspects of plasma features, including ICRF power deposition fraction on thermal ions, q_0 value, fast ion bad orbit power loss and thermal diffusivity. Thermal diffusivity in the plasma core region can be largely enhanced (several times) by ITG and/or TEM turbulence excited by local power deposition. These phenomena will be further compared with the experiment to validate the theoretical transport model. In order to do this, the TRANSP analysis of actual, well diagnosed, future high power experiments will be needed. The scenario development is predicted to improve performance of EAST. It is hoped that this kind of prediction work can help physicists learn the plasma features in advance, and then design their proposals accordingly in the future.

Acknowledgments

The author S Ding would like to thank the TRANSP group at PPPL for their technical support during this study. This work is supported by the National Natural Science Foundation of China under Grant Nos 10725523, 10721505 and 10605028.

References

- [1] Wan B *et al* 2009 *Nucl. Fusion* **49** 104011
- [2] Budny R V *et al* 2008 *Nucl. Fusion* **48** 075005
- [3] Goldston R J *et al* 1981 *J. Comput. Phys.* **43** 61
- [4] Jardin S C, Pomphrey N and Delucia J 1986 *J. Comput. Phys.* **66** 481
- [5] Greenfield C M *et al* 1993 *Plasma Phys. Control. Fusion* **35** B263
- [6] Doyle E J *et al* 2007 *Nucl. Fusion* **47** S18
- [7] LeBlanc B P *et al* 2004 *Nucl. Fusion* **44** 513
- [8] Degtyarev L and Drozdov V 1985 *Comput. Phys. Rep.* **2** 341
- [9] Kinsey J E, Staebler G M and Waltz R E 2005 *Phys. Plasmas* **12** 052503
- [10] Ince-Cushman A *et al* 2009 *Phys. Rev. Lett.* **102** 035002
- [11] Lin Y *et al* 2008 *Phys. Rev. Lett.* **101** 235002
- [12] Waltz R E *et al* 1997 *Phys. Plasmas* **4** 2482
- [13] Bateman G *et al* 1998 *Phys. Plasmas* **5** 1793
- [14] Kritz A H *et al* 2009 *Proc. 36th EPS Conf. on Controlled Fusion Plasma Physics (Sofia, Bulgaria, 29 June–3 July 2009)*
- [15] Bateman G, Onjun T and Kritz A H 2003 *Plasma Phys. Control. Fusion* **45** 1939
- [16] Brambilla M 1999 *Plasma Phys. Control. Fusion* **41** 1
- [17] Ignat D W, Valeo E J and Jardin S C 1994 *Nucl. Fusion* **34** 837